Hydrogen Peroxide Decomposition Rate: A Shock Tube Study Using Tunable Laser Absorption of H_2O near 2.5 μm

Zekai Hong,* Aamir Farooq, Ethan A. Barbour, David F. Davidson, and Ronald K. Hanson

Department of Mechanical Engineering, Stanford University, Stanford, California 94305

Received: July 28, 2009; Revised Manuscript Received: September 16, 2009

The thermal decomposition of hydrogen peroxide was measured behind reflected shock waves in hydrogen peroxide/inert gas mixtures using a sensitive laser diagnostic for water vapor. In these mixtures, the formation rate of water is predominantly controlled by the decomposition rate of hydrogen peroxide. Rate determinations were made over a temperature range of 1000−1200 K and a pressure range of 0.9−3.2 atm for both argon and nitrogen carrier gases. Good detection sensitivity for water was achieved using tunable diode laser absorption of water at 2550.96 nm within its υ_3 fundamental band. Hydrogen peroxide decomposition rates were found to be independent of pressure at 0.9 and 1.7 atm and showed only slight influence of pressure at 3.2 atm. The best fit of the current data to the low-pressure-limit rate for H_2O_2 dissociation in argon bath gas is $k_{1,0} = 10^{15.97\pm0.10}\exp(-21\,220 \pm 250\ \mathrm{K}/T)$ [$\mathrm{cm^3\ mol^{-1}\ s^{-1}}$] (1000−1200 K). Experiments conducted in a nitrogen bath gas show a relative collision efficiency of argon to nitrogen of 0.67.

1. Introduction

The thermal decomposition of hydrogen peroxide (H_2O_2)

$$H_2O_2 + M \rightarrow OH + OH + M \qquad (1)$$

has been identified as the dominant chain-branching reaction that controls hydrocarbon ignition in the intermediate temperature regime (850−1200 K). In fact, to quote Westbrook,[1] the decomposition of hydrogen peroxide is "the central kinetic feature in engine knock in spark ignition engines, in ignition in liquid-fueled diesel engines, and in the operation of homogeneous charge, compression ignition (HCCI) engines". A significant amount of H_2O_2 is accumulated at lower temperatures in the reactive mixture before ignition, followed by the rapid decomposition of H_2O_2 during ignition at temperatures near 1050−1100 K that produces two highly reactive hydroxyl (OH) radicals. Hydrogen peroxide kinetics also plays an important role in the larger problem of peroxy-radical (RO_2) chemistry important in the intermediate temperature oxidation of hydrocarbons.

The decomposition reaction of H_2O_2 has been studied in the temperature range between 700 and 900 K in static cells and flow systems by several research groups.[2−6] However, in the temperature range between 1000 and 1200 K where intermediate temperature hydrocarbon ignition occurs, only a few shock tube studies[7−9] have been carried out, and these were all performed in the same laboratory by Troe and coworkers. In their investigations, the thermal decomposition of H_2O_2 was measured behind reflected shock waves using UV absorption spectroscopy at 215 and 290 nm. These deep UV measurements are influenced by both strongly varying absorption cross sections and interfering species. At 215 nm, HO_2 absorbs much more strongly than H_2O_2;[10,11] therefore, HO_2 reactions as well as the decomposition of H_2O_2 have to be accounted for to interpret the absorbance at 215 nm fully. At 290 nm, HO_2 absorption is negligible, but the poor detection sensitivity of H_2O_2 limits measurement accuracy. The authors of those papers recognized the inherent difficulties in their measurements and have recommended independent studies by other groups.

Attempts have also been made to measure the reverse recombination reaction 1.[12−15] A common approach to study the recombination reaction is to record OH decay after the initial photolysis of OH precursors. However, the recombination reaction 1 on the singlet H_2O_2 potential energy surface competes with reaction 2 on the triplet surface.

$$OH + OH + M \rightarrow H_2O_2 + M \qquad (-1)$$

$$OH + OH \rightarrow H_2O + O \qquad (2)$$

The recombination reaction 1 is pressure-dependent, whereas reaction 2 is not. Theoretically, the rates for reactions 1 and 2 can be distinguished by varying pressure. However, distinguishing between the two reaction rates is difficult, and a factor of three discrepancy exists in the literature for room-temperature measurements of these reactions.[12,13] The interpretation of OH decay profiles in the recombination experiments is further complicated by reactions between OH and interfering species from OH precursors, for example, NO.[15]

Recent advances in infrared (IR) tunable diode lasers have made the two fundamental vibrational bands (υ_1 and υ_3) of water near 2.5 to 3.0 μm accessible. The fundamental bands offer about one order of magnitude enhancement in line strength over the overtone and combination bands previously used by our group for water sensing.[16] The greatly improved water detectivity provides a unique opportunity to investigate the decomposition rate of H_2O_2. During the decomposition of H_2O_2, the formation rate of water is predominantly controlled by the decomposition rate of hydrogen peroxide. Also, because of the mole-for-mole conversion between H_2O_2 and H_2O during the decomposition, an accurate value for the initial H_2O_2 concentration can be inferred from the postshock change in the H_2O concentration. Using this new approach, we have attempted

* Corresponding author. E-mail: hongzk@stanford.edu.

10.1021/jp907219f CCC: $40.75
Published on Web 10/02/2009

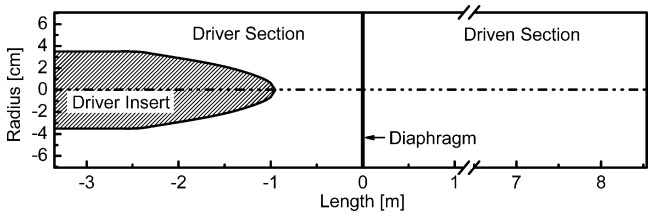

Figure 1. Scale drawing of the driver-insert configuration. After the diaphragm bursts, the incident shock wave propagates from left to right.

to make accurate measurements of the decomposition rate of H_2O_2 over the intermediate temperature range from 1000 to 1200 K.

2. Experimental Setup

2.1. Shock Tube with Modified Driver Section. H_2O_2 thermal decomposition experiments were carried out in a high-purity, 304 stainless steel shock tube with inner diameter of 14.13 cm. The driven section of the shock tube is 8.54 m long, and the driver section is 3.35 m long. The driven section vacuum system consists of a mechanical pump and a Varian V-250 turbomolecular pump to achieve ultimate pressures of 10^{-7} Torr. An ultimate combined leak/outgassing rate of 10^{-6} Torr per minute could typically be achieved with overnight pumping.

Reflected shock conditions were determined using standard normal shock relations. The preshock initial mixture pressure P_1 was measured using a high-accuracy Baratron pressure transducer. Incident shock velocity measurements were made using five piezoelectric pressure transducers (PCB) over the last 1.5 m of the shock tube and four interval counters (Fluke PM6666), and these velocity measurements were linearly extrapolated to the endwall. Average incident shock speed attenuation rates were between 0.5 and 1.5% per meter. Uncertainty in the initial temperature behind the reflected shock wave, T_5, was $\pm 0.8\%$,[17] resulting primarily from the uncertainty in the measured shock speed. In addition to the five PCB pressure transducers for incident shock velocity measurements, another sidewall piezoelectric pressure transducer (Kistler model 603B) located 2 cm from the endwall was used to monitor pressure time histories.

At long test times (e.g., ≥ 3 ms) in typical shock tube experiments, flow variations can increase the uncertainty in temperature significantly. Nonideal effects in shock tubes, such as boundary layer growth, finite diaphragm opening time, and so on are responsible for postreflected-shock pressure/temperature variations at longer times.[18] For the large-diameter shock tube used in this study, a typical pressure rise rate of 2% per millisecond is measured at the observation port 2 cm from the shock tube endwall. Because the test time needed to monitor the entire course of H_2O_2 decomposition near 1000 K is ~ 5 ms, a departure from the normally assumed constant volume model conditions can be as high as 25 K because of these nonideal effects.

To reduce the facility-related effects that cause this increase in pressure and to achieve near-constant pressure and temperature conditions behind reflected shock waves, we have modified the shock tube by inserting a properly designed cone-shaped obstacle into the driver section. A scale drawing of the insert configuration is shown in Figure 1.

A semianalytical model was used to design this shock tube driver insert to eliminate the nonideal pressure rise behind the reflected shock waves.[18] A representative nonreactive example, with pure argon test gas, where the driver insert method has been successfully used to maintain a highly uniform pressure profile for up to 8 ms, is presented in Figure 2. The pressure fluctuation in this example over 8 ms is $\pm 1\%$, which gives an equivalent temperature variation of only $\pm 0.4\%$ (on the basis of an isentropic relation between pressure and temperature in argon). The pressure fluctuations for all of the shocks in the current study are less than $\pm 2\%$, and the corresponding long-time temperature uncertainty is evaluated to be less than $\pm 0.8\%$. These small variations in temperature have been confirmed by in situ temperature measurements.[18]

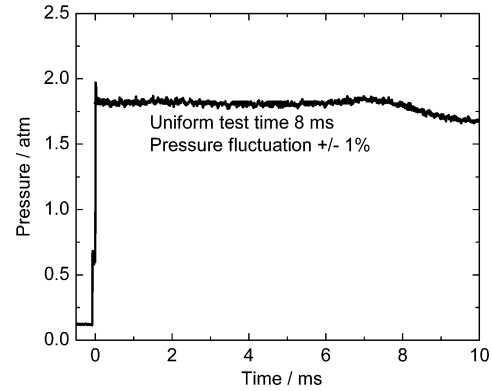

Figure 2. With driver insert, 8 ms of highly uniform test time is obtained for a typical test condition in this study: Ar test gas, $P_5 = 1.83$ atm, $T_5 = 1057$ K.

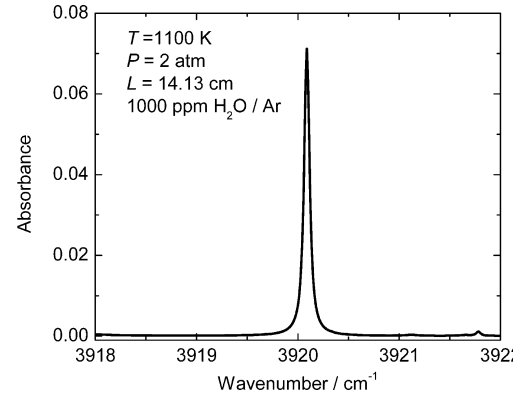

Figure 3. Absorbance spectrum of isolated H_2O vibrational line at 3920.09 cm^{-1}. A small neighboring line is seen near 3922 cm^{-1}.

2.2. Water Diagnostics. The water concentration time histories are measured using tunable diode laser absorption of water at 2550.96 nm (3920.09 cm^{-1}) within the υ_3 fundamental vibrational band. This line is selected primarily because of its large line strength and isolation from nearby lines. As can be seen in Figure 3, the closest water line has a negligibly small line strength and is separated from the line center by 1.7 cm^{-1}. Absorbance in the plot is defined as the product of spectral absorption coefficient k_ν and path length L using Beer's Law, $-\ln(I_\nu/I_\nu^0) = k_\nu L$, where I_ν^0 and I_ν are the incident and transmitted laser intensities, respectively.

The spectral absorption coefficient $k_\nu = S(T)\Phi_\nu P_i$, where $S(T)$ is the temperature-dependent line strength [cm^{-2} atm^{-1}] of the transition at temperature T [K], Φ_ν [cm] is the line-shape function, and P_i is the partial pressure of the absorbing species [atm]. $S(T)$ can be expressed in terms of the line strength at reference temperature $S(T_0)$ as

$$S(T) = S(T_0)\frac{T_0}{T}\frac{Q(T_0)}{Q(T)}\exp\left[-\frac{hcE''}{k}\left(\frac{1}{T}-\frac{1}{T_0}\right)\right]\times \left[1-\exp\left(\frac{-hc\upsilon_0}{kT}\right)\right]\left[1-\exp\left(\frac{-hc\upsilon_0}{kT_0}\right)\right]^{-1}$$

where h [J s] is Planck's constant, c [cm s^{-1}] is the speed of light, k [J K^{-1}] is the Boltzmann constant, υ_0 [cm^{-1}] is the line center frequency, E'' [cm^{-1}] is the lower state energy of the transition, and $Q(T)$ is the rovibrational partition function of the absorbing molecule. In the above equation, the factor $Q(T_0)/Q(T)\exp[-(hcE''/k)((1/T)-(1/T_0))]$ accounts for the temperature-dependent relative change in the equilibrium population fraction of the absorbing molecule in the lower state; $[1-\exp((-hc\upsilon_0)/(kT))][1-\exp((-hc\upsilon_0)/(kT_0))]^{-1}$ for the relative change in induced emission; and T_0/T for the relative change in molecular number density as a function of temperature.

The partition function $Q(T)$ can be obtained from the following polynomial

$$Q(T) = a + bT + cT^2 + dT^3$$

where the coefficients of the polynomial a, b, c, and d are given in HITRAN.[19]

The line-shape function Φ_v is approximated using a Voigt profile characterized by the Doppler broadening coefficient and the collisional broadening coefficient. The collisional broadening coefficient $\gamma(T)$ [cm^{-1} atm^{-1}] (the halfwidth at half-maximum per unit pressure) can be calculated using the following scaling relation with the temperature-dependent coefficient, n

$$\gamma(T) = \gamma(T_0)\left(\frac{T_0}{T}\right)^n$$

In the present study, the parameters for the water feature at 3920.09 cm^{-1}, including $S(T_0)$, E'', and n, were taken from HITRAN.[19] Our analysis shows that the reaction rate determinations are insensitive to the absolute value of k_v, but are controlled by the relative slope of the water time histories; the reaction rate is unchanged even with a 50% error in k_v. In the present study, $\gamma_{N_2}(T_0)$ was approximated by $\gamma_{air}(T_0)$, also given in HITRAN.[19]

The collisional broadening coefficient for argon (not available in HITRAN) was measured in the shock tube over a temperature range between 1000 and 1600 K by matching the peak of the fitted Voigt profile to the measured line center absorbance with a known amount of H_2O and was found to be $\gamma_{Ar}(T) = 0.0277 \times (296/T)^{0.50}$ [cm^{-1} atm^{-1}].

A distributed feedback (DFB) diode laser near 2.5 μm from Nanoplus GmbH was used in this study. The laser wavelength and intensity were controlled by a combination of temperature and injection current using commercial controllers (ILX Lightwave LDT-5910B and LDX-3620). In this study, the laser wavelength was fixed at the center of the water absorption feature. Shortly before taking data, the laser was scanned over the water line to make sure that it was at the line center, as small wavelength drift over time can occur. The typical operating condition for the laser is 20.8 °C and 90 mA, with intensity noise of 0.01% rms.

The laser beam was collimated by a convex lens, transmitted through the shock tube, shielded by a Spectrogon narrow bandpass filter (center wavelength: 2585 ± 10 nm, halfwidth: 35 ± 5 nm), focused by a short-focal-length convex lens into an integrating sphere (SphereOptics SPH-1G-3) to reduce beam-steering effects, and detected by a liquid-nitrogen-cooled InSb detector (IR Associates IS-2.0, 1 MHz bandwidth).

All optical measurements in this work were performed 2 cm from the end wall of the shock tube using sapphire windows. The beam path outside the shock tube was purged with pure N_2 to minimize the laser attenuation due to ambient H_2O.

2.3. H_2O_2 Source. High-temperature gas-phase measurements of the hydroperoxy reaction system are complicated by the highly reactive nature of high-purity H_2O_2 and the lack of a simple H_2O_2 precursor. Commercially available water/H_2O_2 solutions are difficult to use because the vapor pressure of water is significantly higher than that of H_2O_2.[20] Almost all previous researchers had to use high-concentration H_2O_2 solutions (99%) purified by redistillation. Concentrated H_2O_2 is highly volatile and corrosive, and hence a different method to produce H_2O_2 is desired.

An alternative precursor for H_2O_2 is available commercially. The urea−hydrogen peroxide adduct (carbamide peroxide, formula: $(NH_2)_2CO\cdot H_2O_2$) is sold as a solid, is easy to handle, and releases relatively pure hydrogen peroxide gas upon gentle heating (typically to 45 °C). Successful use of this material as a gas-phase H_2O_2 source was demonstrated recently by Ludwig et al.[21]

Urea−hydrogen peroxide adduct (powder, 15−17% active oxygen basis) was provided by Sigma-Aldrich. Approximately 10 g of urea−hydrogen peroxide powder was mixed with roughly an equivalent amount of sand (SiO_2, Sigma-Aldrich) in a polycarbonate flask. The flask was sealed with a platinum-cured silicone stopper and placed in a water bath maintained at 45 °C. The purpose of mixing with sand is to prevent urea−hydrogen peroxide powder from agglomerating upon heating. Research grade argon or nitrogen (99.999%) was passed through the flask at a flow rate of 0.4 to 0.5 SLPM (standard liters per minute) to get a typical H_2O_2 concentration of ~800 ppm. A stable supply of H_2O_2 at this rate can be generated for approximately 3 to 4 h. The H_2O_2/carrier gas mixture was then directed into the driven section of the shock tube from a filling port near the endwall.

To reduce H_2O_2 decomposition on surfaces, the tube and valves downstream of the flask were chosen to have surfaces of either stainless steel (grade 316) or Teflon. H_2O_2 decomposes at accelerated rates when hydrocarbons are present, even in trace amounts; therefore, it was important to remove the residual impurities in the shock tube by passing H_2O_2/carrier gas flow through the length of the driven section of the tube for approximately 20−30 min before taking data.

Despite all of the precautions being taken, H_2O_2 decomposition was still observed in the shock tube with a time constant on the order of 15 min. Previous work[22] has shown that <10% of initially generated H_2O_2 decomposes in the flask at 45 °C. Furthermore, the rate of homogeneous thermal decomposition of H_2O_2 is known to be small. This suggests that the observed H_2O_2 decomposition predominantly takes place on the shock tube wall surfaces. To reduce the decomposition of H_2O_2, it is thus important to minimize the contact time between H_2O_2 vapor and shock tube walls. However, to achieve the desired T_5 and P_5, the corresponding preshock pressure, P_1, was as high as 160 Torr. Given the relatively large volume of the driven section (134 L), a regular filling procedure at a flow rate of 0.4 to 0.5 SLPM required up to 1 h. As a result, an alternative filling strategy was developed to reduce the waiting time significantly: first, fill the entire shock tube with H_2O_2/bath gas mixture to

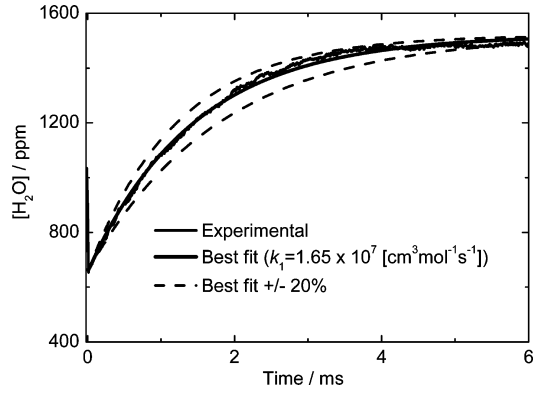

Figure 4. Dissociation rate of H_2O_2 is fitted to be 1.65×10^7 [cm^3 mol^{-1} s^{-1}] with an estimated fitting error of ±10%. Test condition: 860 ppm H_2O_2/663 ppm H_2O/332 ppm O_2/Ar; $P = 1.83$ atm; $T = 1057$ K.

about 10−14 Torr (3 to 4 min); next, bring the shock tube to the target P_1 with pure bath gas using a filling port near the diaphragm location, thereby compressing the initial H_2O_2 mixture into a smaller volume in the test section adjacent to the endwall. We refer to this procedure as staged filling. Because the measurement location (2 cm from endwall) is separated by at least 1 m from the approximate contact region between the initially filled test mixture and the pure argon, we have not observed any irregularities or lack of reproducibility in our data with the filling procedure.

We determined initial H_2O_2 loadings by taking the difference between the initial and final H_2O concentrations. O_2 was also present in the initial mixtures as the other decomposition product of H_2O_2. The initial O_2 concentrations were assumed to be half of the initial H_2O concentrations. Numerical simulations using the chemical kinetics model GRI-Mech 3.0[23] suggest that the presence of H_2O and O_2 in the test gas mixture only affects average collider efficiency. Although the efficiency of H_2O is perhaps 10 times larger than that of N_2, 500 ppm of H_2O (and 250 ppm O_2) introduces <1% uncertainty in the determination of the H_2O_2 decomposition rate in an argon diluent.

3. Results and Discussion

3.1. Determination of H_2O_2 Dissociation Rate, k_1. In the present study, the dissociation rate, k_1, is defined as the second-order rate of reaction 1. Time histories of water absorbance at the line center were converted into water concentrations using spectroscopy data discussed in Section 2.2. Figure 4 shows an example water concentration profile recorded at 1057 K and 1.83 atm in an argon bath gas. Water concentrations at time zero and in the plateau region at late times are 663 and 1523 ppm, respectively, corresponding to a water yield of 860 ppm. Considering that the overall reaction of H_2O_2 decomposition can be described by

$$H_2O_2 = H_2O + 1/2O_2$$

the initial H_2O_2 loading is inferred to be 860 ppm.

Using a detailed chemical kinetics mechanism, GRI-Mech 3.0,[23] we calculated water sensitivity coefficients with the Senkin[24] kinetics code package. The sensitivity coefficient α is the partial derivative of a species mole fraction with respect to the rate constant parameter A of a reaction, normalized by the maximum species mole fraction and the rate constant parameter A

$$\alpha_{ij}(t) = (dX_j/X_j^{max})/(dA_i/A_i)$$

where X_j is the mole fraction of species j and A_i is the temperature-independent factor of the rate constant of reaction i. Figure 5 is the water sensitivity plot for conditions of Figure 4, showing that H_2O formation is predominantly controlled by k_1. No other reactions show sensitivity at a noticeable level using GRI-Mech 3.0. Therefore, k_1 can be determined simply by changing this rate in the chemical kinetics model to best fit experimental water time histories. The best-fit dissociation rate for the example case is 1.65×10^7 [cm^3 mol^{-1} s^{-1}] with an estimated fitting error of less than ±10% (Figure 4).

In addition to the fitting uncertainty, uncertainty in temperature is the other major source of error. As discussed in Section 2.1, the initial temperature T_5 immediately behind the reflected shock wave is determined from the measured incident shock speed, and the uncertainty is estimated to be ±8 K. The long-time temperature uncertainty is evaluated to be less than ±0.8%, or ±8 K. The combined uncertainty in temperature is estimated to be ±11 K, resulting in an associated uncertainty in the measured reaction rate of ±21%.

The decomposition rate of H_2O_2 is inferred essentially from the relative slope of the H_2O formation profile. Therefore, uncertainty in the H_2O absorption cross-section does not significantly affect the accuracy of this measurement. Combining uncertainties in fitting and temperature, we estimate the overall uncertainty in k_1 to be ±23%.

3.2. Low-Pressure Limit and Falloff Behavior in Argon Bath Gas. Experimentally measured k_1 data in argon bath gas at 0.9, 1.7, and 3.2 atm are provided in Table 1. Best fits of experimental determinations of k_1 at various pressures yield the following expressions

$$k_1(M = Ar, 0.9\ atm) = 10^{16.12\pm0.09} \exp(-21\,650 \pm 230\ K/T)\ [cm^3\ mol^{-1}\ s^{-1}]$$

$$k_1(M = Ar, 1.7\ atm) = 10^{15.92\pm0.13} \exp(-21\,060 \pm 320\ K/T)\ [cm^3\ mol^{-1}\ s^{-1}]$$

$$k_1(M = Ar, 3.2\ atm) = 10^{15.75\pm0.15} \exp(-20\,770 \pm 380\ K/T)\ [cm^3\ mol^{-1}\ s^{-1}]$$

The results are also summarized in an Arrhenius plot. (See Figure 6.) Good agreement is seen between this study and that of Kappel et al.[9]

The reduced experimental scatter in the present study, relative to past studies, enables an evaluation of the pressure dependence of k_1. The comparison of the measurements at 0.9 and 1.7 atm does not show deviation from second-order behavior, suggesting that the dissociation reaction of H_2O_2 is essentially at its low-pressure limit at pressures <1.7 atm. A best fit to all data obtained at 0.9 and 1.7 atm yields the low-pressure limit in argon to be $k_{1,0} = 10^{15.97\pm0.10} \exp(-21\,220 \pm 250\ K/T)$ [cm^3 mol^{-1} s^{-1}] over the temperature range of 1000−1200 K.

Recently, Sellevåg et al.[25] calculated the high-pressure limit rate of H_2O_2 decomposition using variable reaction coordinate transition-state theory, classical trajectory simulations, and a two-transition-state model. They also analyzed the experimental data by Kappel et al.[9] to obtain the energy transfer parameter ΔE_d with argon as the bath gas. Using a two-dimensional master equation (2D-ME), the low-pressure limit of the reaction was calculated. Their result is compared with the experimental data

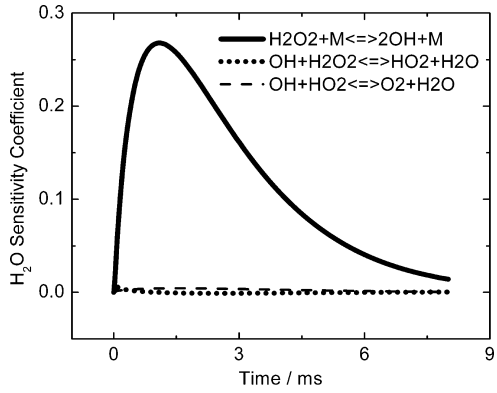

Figure 5. Formation of H_2O is predominantly controlled by the dissociation rate of H_2O_2. Conditions are those of Figure 4.

TABLE 1: Test Conditions and Results of H_2O_2 Decomposition Experiments in Argon Bath Gas[a]

T (K)	P (atm)	[H_2O] (ppm)	[H_2O_2] (ppm)	k_1 (cm^3 mol^{-1} s^{-1})
1077	1.776	560	850	2.50×10^7
1020	1.698	498	512	9.50×10^6
1085	1.845	346	280	2.90×10^7
1067	1.813	363	261	2.30×10^7
1100	1.757	561	748	4.15×10^7
1120	1.738	410	874	5.50×10^7
1124	1.717	434	796	6.40×10^7
1139	1.708	438	505	8.00×10^7
1157	1.705	453	613	1.05×10^8
1167	1.676	390	551	1.20×10^8
1169	1.626	394	436	1.30×10^8
1065	1.811	522	900	1.90×10^7
1190	1.663	432	753	1.80×10^8
1204	1.64	315	367	2.10×10^8
1029	1.667	1530	480	1.10×10^7
1057	1.831	663	860	1.60×10^7
1047	1.857	639	838	1.50×10^7
1009	1.776	447	853	8.20×10^6
1054	1.663	473	851	1.70×10^7
1132	1.721	373	605	6.80×10^7
1095	1.78	303	574	3.27×10^7
1170	1.656	403	775	1.20×10^8
1100	3.133	471	710	3.50×10^7
1115	3.089	435	772	4.50×10^7
1129	2.997	440	717	5.70×10^7
1154	2.964	454	769	8.30×10^7
1182	2.935	411	713	1.43×10^8
1075	3.186	670	860	2.30×10^7
1057	3.262	658	745	1.70×10^7
1036	3.309	400	773	1.05×10^7
1016	3.352	437	1058	8.00×10^6
1101	0.901	372	625	4.10×10^7
1123	0.877	356	840	5.70×10^7
1163	0.867	191	744	1.05×10^8
1183	0.856	370	1422	1.49×10^8
1216	0.85	440	1459	2.50×10^8
1081	0.934	500	1160	2.60×10^7
1065	0.974	372	1116	1.89×10^7
1030	0.977	431	932	1.00×10^7
1038	0.98	424	1094	1.16×10^7

[a] H_2O_2 and H_2O concentrations are initial values.

in Figure 6. The limiting low-pressure rate recommended by Sellevåg et al. over the temperature range of 1000−1200 K can be approximated by a two-parameter Arrhenius formula $k_{1,0} = 10^{16.01} \exp(-21\,230\ \mathrm{K}/T)$ [cm^3 mol^{-1} s^{-1}], which is in excellent agreement with the experimental measurements of the present work. At 3.2 atm, a small reduction (∼10%) in k_1 from the proposed low-pressure limit rate, $k_{1,0}$, was observed. However, the experimental uncertainty of 23% prevents a more definite

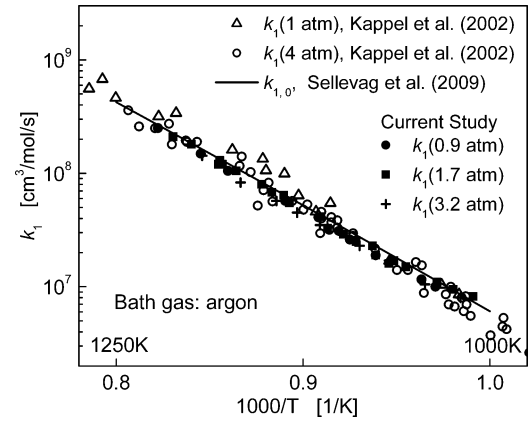

Figure 6. Decomposition rates of H_2O_2 (k_1) in argon bath gas were measured at various pressures and are compared with previous studies.

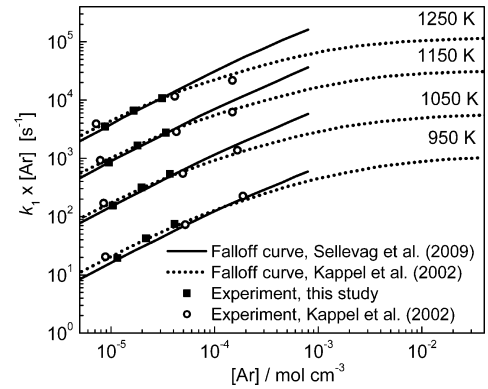

Figure 7. Falloff behavior of H_2O_2 decomposition in argon bath gas.

conclusion on pressure falloff to be drawn. Experiments conducted at much higher pressures are needed to evaluate the falloff curve because there are no existing direct measurements of the H_2O_2 dissociation rate near the high-pressure limit.

Sellevåg et al.[25] also calculated the falloff curves for the decomposition of H_2O_2 in argon near its low-pressure limit, as plotted in Figure 7. Although Sellevåg et al. extracted ΔE_d from the study by Kappel et al.,[9] they found that "the experimental data seem to fall off faster systematically from the low-pressure limit than can be explained by (their) 2D-ME calculations". Using the best-fits to experimental results at 0.9, 1.7, and 3.2 atm from this study, the falloff behavior at various temperatures can be estimated at corresponding pressures. The comparison between the experimental data and the theoretical curves shows excellent agreement, confirming the observed second-order reaction behavior.

The falloff curves in argon have also been estimated by Kappel et al.[9] on the basis of their measurements made at 1, 4, and 15 atm. The authors acknowledged the uncertainties inherent in their falloff curves, predominantly because of the lack of data near the high-pressure limit and to their experimental scatter. Their falloff curves suggest that the departure from the low-pressure limit occurs at much lower pressures. The extrapolated $k_{1,\infty}$ from the Kappel et al. falloff curves fall about a factor of 10 below the recent theoretical predictions by Troe and Ushakov.[26] That theoretical calculation of $k_{1,\infty}$[26] is supported by the only existing set of high-pressure (150 bar) recombination measurements;[14] the agreement is within a factor of two. The high-pressure rates were obtained in hydroxyl recombination experiments conducted at room temperature. Although the

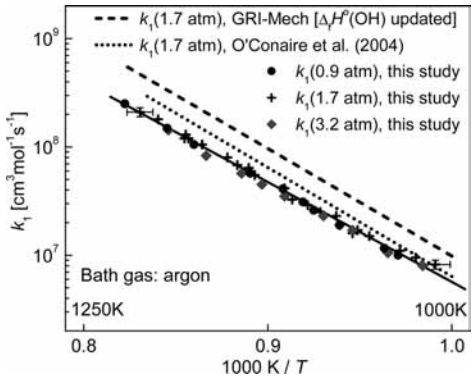

Figure 8. Comparison between the rate expressions used in two detailed chemical kinetics models and the experimental data of this study (long dashed line, GRI-Mech with $\Delta_f H°$(OH) updated; short dotted line, Ó Conaire et al.; solid line, the limiting low-pressure rate fitted to the experimental data at 0.9 and 1.7 atm of this study).

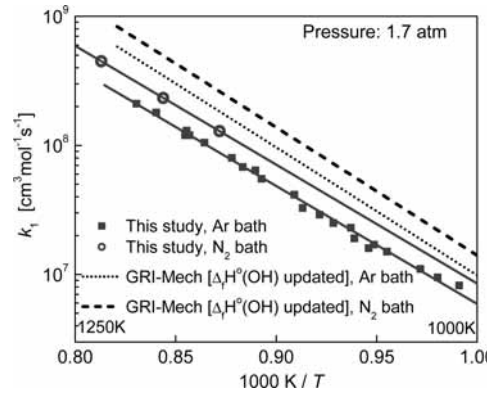

Figure 9. Decomposition rates of H_2O_2 (k_1) in nitrogen bath gas are compared with the results obtained in argon at the same pressure. Solid lines are the best fits. Dotted lines are model predictions.

dissociation rates k_1 inferred from recombination experiments are less accurate because of the competition from the interference reaction 2, they confirm our observation that there is only small departure from the low-pressure limit at 3.2 atm.

The measured H_2O_2 decomposition rates are also compared with the predictions of two detailed chemical kinetics models in Figure 8. The decomposition rate of H_2O_2 used in the Ó Conaire et al. model[27] is based on Baulch et al.'s review of k_1[28] and the theoretical study by Brouwer et al.[29] In GRI-Mech 3.0,[23] the rate is given in the reverse direction (k_{-1}) on the basis of the Baulch et al. review of k_{-1}[30] and a hydroxyl recombination experiment by Zellner et al.[13] From k_{-1}, the corresponding k_1 can be inferred from the relationship through the equilibrium constant $K_c = k_1/k_{-1}$ using a heat of formation of H_2O_2 of $\Delta_f H°_{298}(H_2O_2) = -32.49 \pm 0.04$ kcal/mol.[23,27,31] $\Delta_f H°_{298}$(OH) has been updated from 9.40 to 8.91 kcal/mol by Herbon et al.[32] and Ruscic et al.[33] K_c can be formulated to be $K_c = 106.44 \exp(-24\,685\ \mathrm{K}/T)$ [cm^{-3} mol] in the temperature range of 1000−1200 K. The comparisons suggest that the rate expressions used in both kinetics models (GRI-Mech and Ó Conaire et al.) are larger than the current results and would therefore overpredict the rate of H_2O_2 thermal decomposition, whereas the recent calculations by Sellevåg et al.[25] show much better agreement (Figure 6).

3.3. Collider Efficiencies. For most practical combustion studies, nitrogen is the most significant collision partner. The difference in collider efficiency between argon and nitrogen was therefore examined. Similar H_2O_2 decomposition experiments were conducted in nitrogen bath gas at pressures near 1.7 atm.

Accurate determinations of the temperatures in shock tube experiments with nitrogen are more complicated, however, owing to vibrational relaxation processes. Nitrogen molecules undergo vibrational relaxation[34] behind shock waves to reestablish the equilibrium between vibrational and translational/rotational modes. The process can be characterized by two limiting temperatures: (1) frozen temperature: the temperature of translational/rotational modes before any vibrational relaxation has taken place and (2) equilibrium temperature: the temperature when the molecule is fully vibrationally relaxed. To decide which temperature most accurately describes the chemical kinetics processes, the characteristic times of vibrational relaxation, τ_{V-T}, were compared with the corresponding characteristic times of H_2O_2 decomposition, τ_{decomp}.

The characteristic times of vibrational relaxation τ_{V-T} for the test mixtures in the present study can be estimated using the relation

$$\frac{1}{\tau_{V-T}} = \frac{\Phi_{N_2}}{\tau_{N_2-N_2}} + \frac{\Phi_{H_2O}}{\tau_{N_2-H_2O}} + \frac{\Phi_{H_2O_2}}{\tau_{N_2-H_2O_2}}$$

as suggested by Millikan and White,[34] where Φ_X is the mole fraction of the collision partner X and τ_{N_2-X} is the characteristic time of vibrational relaxation of N_2 by X. $\tau_{N_2-N_2}$ and $\tau_{N_2-H_2O}$ can be evaluated under corresponding test conditions using the correlations given in the references.[34,35] However, no data were found for $\tau_{N_2-H_2O_2}$, and it was approximated by $\tau_{N_2-H_2O}$ because of the similarities in molecular structure and composition. The estimated τ_{V-T} values, along with the corresponding τ_{decomp}, are listed in Table 2.

However, the two characteristic times are comparable, except for tests conducted near the high-temperature extreme of the present study, where the decomposition of H_2O_2 is significantly faster than the vibrational relaxation of N_2 ($\tau_{V-T}/\tau_{decomp} > 2$). Therefore, the temperatures at which these tests were evaluated are best approximated by the vibrationally frozen temperature and are shown in the Arrhenius plot in Figure 9. The collider efficiency of argon relative to nitrogen was found to be 0.67. Previous low-temperature (<850 K) flow reactor experiments[2] reported a relative efficiency of 0.67 for argon bath gas, which is in excellent agreement with the findings of this study.

4. Conclusions

The decomposition rate of H_2O_2 was studied behind reflected shock waves over the temperature range between 1000 and 1200 K using laser absorption spectroscopy of water at 2550.96 nm.

TABLE 2: Test Conditions and Results of H_2O_2 Decomposition Experiments in Nitrogen Bath Gas[a]

T_{frozen} (K)	$T_{equilbrium}$ (K)	P (atm)	[H_2O] (ppm)	[H_2O_2] (ppm)	τ_{V-T} (milliseconds)	τ_{decomp} (milliseconds)	τ_{V-T}/τ_{decomp}	k_1 (cm^3 mol^{-1} s^{-1})
1147	1089	1.485	531	1474	0.626	0.306	2.05	1.29×10^{08}
1185	1122	1.448	416	1800	0.567	0.177	3.20	2.33×10^{08}
1230	1154	1.413	390	1675	0.600	0.101	5.94	4.49×10^{08}

[a] H_2O_2 and H_2O concentrations are initial values.

We determined the decomposition rates of H_2O_2 by fitting the measured water profiles, and they were not significantly influenced by competing reactions. Agreement with previous studies by Troe and coworkers is very good. No pressure dependence of the decomposition rate was resolved between 0.9 and 1.7 atm in argon. At 3.2 atm, a ~10% deviation from these lower-pressure measurements was observed. The low-pressure reaction rate was inferred from these measurements and found to be $k_{1,0} = 10^{15.97\pm0.10} \exp(-21\,220 \pm 250\ \mathrm{K}/T)$ [$\mathrm{cm^3\ mol^{-1}\ s^{-1}}$] (1000−1200 K). The collider efficiency of argon relative to nitrogen was experimentally determined to be 0.67, which is in excellent agreement with low temperature experiments conducted in a flow reactor.[2]

Acknowledgment. This work was supported by the National Science Foundation with Dr. Phillip Westmoreland as technical monitor. We are grateful to Prof. David M. Golden at Stanford University for helpful discussions.

References and Notes

(1) Westbrook, C. Chemical Kinetics of Hydrocarbon Ignition in Practical Combustion Systems. *Proc. Combust. Inst.* **2000**, *28*, 1563−1577.

(2) Baldwin, R. R.; Brattan, D. Homogeneous Gas-Phase Decomposition of Hydrogen Peroxide. *Proc. Combust. Inst.* **1991**, *8*, 110–119.

(3) McLane, C. K. Hydrogen Peroxide in the Thermal Hydrogen−Oxygen Reaction. I. Thermal Decomposition of Hydrogen Peroxide. *J. Chem. Phys.* **1949**, *17*, 379–385.

(4) Satterfield, C. N.; Stein, T. W. Homogeneous Decomposition of Hydrogen Peroxide Vapor. *J. Phys. Chem.* **1957**, *61*, 537–540.

(5) Forst, W. Second-Order Unimolecular Kinetics in the Thermal Decomposition of Hydrogen Peroxide Vapor. *Can. J. Chem.* **1958**, *36*, 1308–1319.

(6) Hoare, D. E.; Protheroe, J. B.; Walsh, A. D. The Thermal Decomposition of Hydrogen Peroxide Vapour. *Trans. Faraday Soc.* **1959**, *55*, 548–557.

(7) Meyer, E.; Olschewski, H. A.; Troe, J.; Wagner, H. Gg. Investigation of N_2H_4 and H_2O_2 Decomposition in Low and High Pressure Shock Waves. *Proc. Combust. Inst.* **1969**, *12*, 345–355.

(8) Kijewski, H.; Troe, J. Study of the Pyrolysis of H_2O_2 in the Presence of H_2 and CO by Use of UV Absorption of HO_2. *Int. J. Chem. Kinet.* **1971**, *3*, 223–235.

(9) Kappel, Ch.; Luther, K.; Troe, J. Shock Wave Study of the Unimolecular Dissociation of H_2O_2 in its Falloff Range and of Its Secondary Reactions. *Phys. Chem. Chem. Phys.* **2002**, *4*, 4392–4398.

(10) Kijewski, H.; Troe, J. Temperature Dependence of the Ultraviolet Spectra of H_2O_2 and HO_2 radicals. *Helv. Chim. Acta* **1972**, *55*, 205–213.

(11) Nielsen, O. J.; Johnson, M. S.; Wallington, T. J.; Christensen, L. K.; Platz, J. UV Absorption Spectra of HO_2, CH_3O_2, $C_2H_5O_2$, and $CH_3C(O)CH_2O_2$ Radicals and Mechanism of the Reactions of F and Cl Atoms with $CH_3C(O)CH_3$. *Int. J. Chem. Kinet.* **2002**, *34*, 283–291.

(12) Trainor, D. W.; von Rosenberg, C. W., Jr. Flash Photolysis Study of the Gas Phase Recombination of Hydroxyl Radicals. *J. Chem. Phys.* **1974**, *61*, 1010–1015.

(13) Zellner, R.; Ewig, F.; Paschke, R.; Wagner, G. Pressure and Temperature Dependence of the Gas-Phase Recombination of Hydroxyl Radicals. *J. Phys. Chem.* **1988**, *92*, 4184–4190.

(14) Forster, R.; Frost, M.; Fulle, D.; Hamann, H. F.; Hippler, H.; Schlepegrell, A.; Troe, J. High Pressure Range of the Addition of HO to HO, NO, NO_2, and CO. I. Saturated Laser Induced Fluorescence Measurements at 298 K. *J. Chem. Phys.* **1995**, *103*, 2949–2958.

(15) Fulle, D.; Hamann, H. F.; Hippler, H.; Troe, J. High-Pressure Range of the Addition of HO to HO. III. Saturated Laser-Induced Fluorescence Measurements between 200 and 700 K. *J. Chem. Phys.* **1996**, *105*, 1001–1006.

(16) Farooq, A.; Jeffries, J. B.; Hanson, R. K. In situ Combustion Measurements of H_2O and Temperature near 2.5 μm Using Tunable Diode Laser Absorption. *Meas. Sci. Technol.* **2008**, *19*, 1–11.

(17) Herbon, J. T. Shock Tube Measurements of $CH_3 + O_2$ Kinetics and the Heat of Formation of the OH Radical. Ph.D. Dissertation, Stanford University, Stanford, CA, 2004. http://thermosciences.stanford.edu/pdf/TSD−153.pdf (accessed June 15, 2009).

(18) Hong, Z.; Pang, G. A.; Vasu, S. S.; Davidson, D. F.; Hanson, R. K. The Use of Driver Inserts to Reduce Non-Ideal Pressure Variations behind Reflected Shock Waves. *Shock Waves* **2009**, *19*, 113–123.

(19) Goldman, A.; Gamache, R. R.; Perrin, A.; Flaud, J. M.; Rinsland, C. P.; Rothman, L. S. 2000 HITRAN Partition Functions and Weighed Transition-Moments Squared. *J. Quant. Spectrosc. Radiat. Transfer* **2000**, *66*, 455–486.

(20) Van Laar, J. J. Uber Dampfspannungen von Binaren Gemischen. *Z. Phys. Chem.* **1910**, *72*, 723–751.

(21) Ludwig, W.; Brandt, B.; Friedrichs, G.; Temps, F. Kinetics of the Reaction $C_2H_5 + HO_2$ by Time-Resolved Mass Spectrometry. *J. Phys. Chem. A* **2006**, *110*, 3330–3337.

(22) Ludwig, W. Kinetics of the Reaction $C_2H_5 + HO_2$ by Time-Resolved Mass Spectrometry. Ph.D. Dissertation, Institut für Physikalische Chemie, Christian-Albrechts-Universität zu Kiel, Kiel, Germany, 2004.

(23) Smith, G. P.; Golden, D. M.; Frenklach, M.; Moriarty, N. W.; Eiteneer, B.; Goldenberg, M.; Bowman, C. T.; Hanson, R. K.; Song, S.; Gardiner, W. C.; Lissianski, V. V.; Qin, Z. *GRI-Mech 3.0*. http://www.me.berkeley.edu/grimech/ (accessed March 12, 2009).

(24) Lutz, A. E.; Kee, R. J.; Miller, J. A. *Senkin: A FORTRAN Program for Predicting Homogeneous Gas Phase Chemical Kinetics with Sensitivity Analysis*; Report No. SAND87-8248; Sandia National Laboratory: Albuquerque, NM, 1988.

(25) Sellevåg, S. R.; Georgievskii, Y.; Miller, J. A. Kinetics of the Gas-Phase Recombination Reaction of Hydroxyl Radicals to Form Hydrogen Peroxide. *J. Phys. Chem. A* **2009**, *113*, 4457–4467.

(26) Troe, J.; Ushakov, V. G. SACM/CT Study of the Dissociation/Recombination Dynamics of Hydrogen Peroxide on an Ab Initio Potential Energy Surface: Part II. Specific Rate Constants $k(E,J)$, Thermal Rate Constants $k_\infty(T)$, and Lifetime Distributions. *Phys. Chem. Chem. Phys.* **2008**, *10*, 3915–3924.

(27) Ó Conaire, M.; Curran, H. J.; Simmie, J. M.; Pitz, W. J.; Westbrook, C. K. A Comprehensive Modelling Study of Hydrogen Oxidation. *Intl. J. Chem. Kinet.* **2004**, *36*, 603–622.

(28) Baulch, D. L.; Drysdale, D. D.; Horne, D. G.; Lloyd, A. C. *Evaluated Kinetic Data for High Temperature Reactions: Homogeneous Gas Phase Reactions of the H_2-O_2 System*; Butterworths,: London, 1972; Vol. 1.

(29) Bouwer, L.; Cobos, C. J.; Troe, J.; Dübal, H.-R.; Crim, F. F. Specific Rate Constants $k(E,J)$ and Product Stat Distributions in Simple Bond Fission Reactions. II. Application to HOOH → OH + OH. *J. Chem. Phys.* **1987**, *86*, 6171–6182.

(30) Baulch, D. L.; Cobos, C. J.; Cox, R. A.; Esser, C.; Frank, P.; Just, Th.; Kerr, J. A.; Pilling, M. J.; Troe, J.; Walker, R. W.; Warnatz, J. J. *J. Phys. Chem. Ref. Data* **1992**, *21*, 411.

(31) Burcat, A.; Ruscic, B. *Third Millennium Ideal Gas and Condensed Phase: Thermochemical Database for Combustion*; Joint Argonne National Laboratories Report ANL-05/20 and a Technion Aerospace Report TAE 960; Argonne, IL, 2005.

(32) Herbon, J. T.; Hanson, R. K.; Golden, D. M.; Bowman, C. T. A Shock Tube Study of the Enthalpy of Formation of OH. *Proc. Combust. Inst.* **2003**, *29*, 1201–1208.

(33) Ruscic, B.; Wagner, A. F.; Harding, L. B.; Asher, R. L.; Feller, D.; Dixon, D. A.; Peterson, K. A.; Song, Y.; Qian, X. M.; Ng, C. Y.; Liu, J. B.; Chen, W. W. On the Enthalpy of Formation of Hydroxyl Radical and Gas-Phase Bond Dissociation Energies of Water and Hydroxyl. *J. Phys. Chem. A* **2002**, *106*, 2727–2747.

(34) Millikan, R. C.; White, D. R. Systematic of Vibrational Relaxation. *J. Chem. Phys.* **1963**, *39*, 3209–3213.

(35) Center, R. E.; Newton, J. F. Vibrational Relaxation of N_2 by H_2O. *J. Chem. Phys.* **1978**, *68*, 3327–3333.

JP907219F